Hindawi
International Journal of Antennas and Propagation
Volume 2023, Article ID 2729945, 9 pages
https://doi.org/10.1155/2023/2729945

Research Article

Shaped Omnidirectional Reflector Fed by a Dielectric Lens Associated with a Coaxial Feed Horn

J. R. Bergmann and L. S. Patinos

CETUC–Center for Telecommunications Studies, PUC-Rio-Pontifical Catholic University of Rio de Janeiro, Rio de Janeiro, RJ 22453-900, Brazil

Correspondence should be addressed to J. R. Bergmann; bergmann@puc-rio.br

Received 31 October 2022; Revised 25 January 2023; Accepted 10 May 2023; Published 23 May 2023

Academic Editor: Miguel Ferrando Bataller

The paper explores an omnidirectional antenna configuration composed of a reflector fed by a shaped dielectric lens associated with a coaxial TEM horn. A simple formula describes the lens shape obtained by applying Fermat's principle to control the rays' caustic emerging from the dielectric interface. Based on geometrical optics (GO) principles, a synthesis technique defines the reflector shape to control the antenna radiation pattern in the vertical plane. Concatenated conic describes the reflector generatrix. The study employs a full-wave analysis to validate the designs and explores the proposed configuration to attend two distinct far-field specifications.

1. Introduction

For operation in millimeter waves, shaped omnidirectional reflector antennas can provide efficient anikd broadband communications with compact configurations. Design examples with a single and dual reflector have been explored for omnidirectional coverages [1–5]. These antenna design examples are usually fed by a small aperture horn that generates radiation patterns with large beamwidth [1–2]. Consequently, a single reflector configuration requires reflectors with large diameters to minimize the spillover effects. Dual classical geometries successfully control peak radiation patterns and provide compact solutions [4, 5]. One of the major features of a dual omnidirectional configuration is the possibility of adjusting the position of the real or virtual caustic generated by the subreflector to minimize the main reflector diameter, leading to more compact designs when compared with the single case with a similar aperture size [3]. Based on geometrical optics principles, the authors in [4, 5] show a shaping procedure for omnidirectional dual reflector antennas where an axis-displaced conical section describes desubreflector and the main reflector GO shape controls the radiation pattern in the vertical plane. They show configurations that differ by the ray structure emerging from the main reflector, presenting a real or a virtual caustic. For both cases, the value for grazing incidence on the main reflector for rays emerging from the subreflector and the conditions for main reflector blockage limit the large-angle coverages. As observed for the virtual caustic case, the coverage angle and the shaping increase the main reflector dimensions.

Dielectric lenses associated with a primary feed offer the advantages of mechanical rigidity, wide-band capabilities, and low dissipative loss. For single surface-lenses, their profile can be either canonical or shaped to satisfy far-field radiation pattern specifications [6–8]. The usual shaping techniques based on geometric optics (GO) principles are formulated by imposing a power conservation on a ray tube and the Snell refraction law to control the lens radiation pattern [7–9]. Alternatively, the lens shape can also be obtained by applying Fermat's principle to control the rays' caustic emerging from the dielectric interface [10].

For operation in local multipoint distribution services in millimeter waves at 30 GHz, here, we explore an alternative configuration for omnidirectional antennas where a circularly symmetric dielectric lens illuminates a circularly

symmetric main reflector, as illustrated in Figure 1. A TEM coaxial horn feeds the lens and provides vertical polarization. The antenna radiation pattern in the vertical plane is obtained by applying a shaping technique based on GO assumptions and considering the system horn-lens as a point source at a virtual focus. The rays emerging from the shaped lens interface creates a virtual focus behind the feed, narrows the lens radiation pattern that illuminates the reflector, and reduces the required reflector diameter and, consequently, the antenna's overall volume. Compared with the dual configurations, the reflector on the top of the lens avoids the grazing incidence and allows a large coverage angle without blockage. The material is presented as follows: Section 2 offers a simple formula to describe the lens generatrix based on Fermat's principle and the lens radiation pattern. Section 3 presents the GO reflector shaping method assuming the new virtual feed focus. The resulting reflector generatrix is represented by concatenated local conic sections [11]. Section 4 presents two design examples that are validated by employing the full-wave analysis provided by the CST Studio Suite.

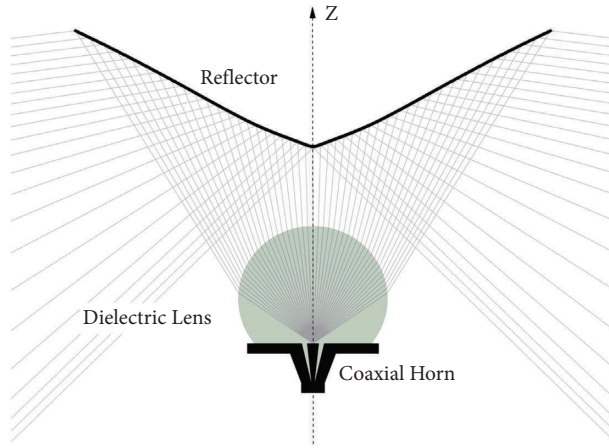

Figure 1: General view of the antenna: reflector, lens, and horn.

2. Lens Design

Figure 2 shows the basic dimensions of the circularly symmetric dielectric lens fed by a point source at the origin O of the Cartesian system. The base of the dielectric lens is planar and coincides with the plane $z = 0$. The lens dimensions are larger than the wavelength, and we used GO approximations to shape the lens and produce a spherical wavefront with a center at the virtual focus at $P(0, -Z_0)$. By applying Fermat's principle to the ray path from the source point at the origin to the dielectric interface, the distance $r_0(\theta)$ has to satisfy the following equation:

$$\mathrm{r}_0(\theta)n - \mathrm{r}_p(\theta) = c, \tag{1}$$

where $r_0(\theta)$ *e* $r_p(\theta)$ are the distance of the point S on the interface to the points O and P, respectively, n is the refraction index of the dielectric, Z_A defines the size of the lens along the symmetry axis (z axis), and $c = Z_A(n-1) - Z_0$. The

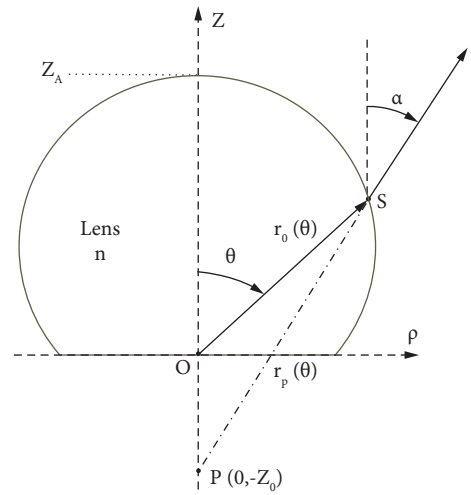

Figure 2: Lens geometry.

solution of (1) leads to the following expression for the generatrix of the dielectric-air interface (see Appendix 1):

$$r_o(\theta) = \frac{nc + Z_0\cos(\theta)}{\left(n^2 - 1\right)} + \frac{\sqrt{c^2 + Z_0^2\left(n^2 - \sin^2(\theta)\right) + 2ncZ_0\cos(\theta)}}{\left(n^2 - 1\right)}. \tag{2}$$

The lens surface is circularly symmetric and obtained by rotating the generatrix around the Z-axis, the antenna symmetry axis. The direction of the incident ray and refracted rays is related as follows:

$$\alpha(\theta) = \tan^{-1}\left[\frac{r_0(\theta)\sin(\theta)}{r_0(\theta)\cos(\theta) + Z_0}\right]. \tag{3}$$

The desire for a compact lens requires the reduction of Z_A, bringing, as a consequence, the increase of the surface curvature and total reflections of the rays incident at a larger angle ($\theta > \theta_C$). To avoid this limitation, Z_A has to satisfy the following condition $Z_A > Z_0/(n\,1)$.

The GO reflector synthesis supposes the reflector is illuminated by a spherical wave with a phase center at P and requires an analytical representation of the radiation intensity $G_L(\alpha)$. By applying the power conservation principle along an elementary ray tube, $G_L(\alpha)$ can be expressed by comparing the transmitted power from the source point to an elementary external surface of the lens in the direction θ with the power radiated in the direction α, yielding:

$$G_L(\alpha) = T(\theta) I(\theta) \left[\frac{\sin(\theta)}{\sin(\alpha)}\right] \frac{d\theta}{d\alpha}, \quad (4)$$

where $T(\theta)$ is ratio of the transmitted power to the incident one on the interface

$$T(\theta) = \left[1 - R^2\right] \left[\frac{\cos(\theta_i)}{\cos(\theta_t)}\right], \quad (5)$$

and R is the Fresnel local reflection coefficient for the parallel component of the incident electric field [8].

To illustrate the lens performance, we chose a TEM coaxial horn with dimensions similar to the design described in [12]. We considered it immersed in the dielectric material employed for the lens (dielectric constant is $\varepsilon = 2.56$ and $n = 1.56$), as shown in Figure 3. Consequently, the horn has internal and external aperture radii $r_a = 0.45\lambda_d = 0.2815$ cm and $r_b = 0.9\lambda_d = 0.5625$ cm, respectively, where λ_d is the wavelength inside the dielectric (see Figure 2 in [12]). As the aperture dimension is relatively small, the phase center of the horn's far-zone radiation is very close to the origin O, at the plane $z = 0$, as supposed in the formulation. The horn radiation pattern model is expressed as follows:

$$I(\theta) = G_F \left[\frac{J_0(k_d r_a \sin(\theta)) - J_0(k_d r_b \sin(\theta))}{\sin(\theta)}\right]^2, \quad (6)$$

where G_F is the normalization factor, $J_0(.)$ is the Bessel of order zero, and k_d is the wave number inside the dielectric (see Appendix 2). Figure 4 shows the CST horn radiation pattern in the absence of the lens interface and compares it with the model described by (6).

The lens design supposes the rays emerging from the lens interface with a virtual focal point at $Z_0 = 3.5$ cm on the symmetry axis. To avoid any critical incidence on the interface, the lens size $Z_A = 6$ cm is adjusted to satisfy the condition $Z_A > Z_0/(n\,1)$. These lens dimensions make the rays radiated in the semispace $z > 0$ and concentrate in the solid angle defined by $\alpha < 39.6^\circ$, reducing the width of the main lobe, as illustrated the GO radiation in Figure 5. The diameter of the metallic base in the plane $z = 0$ is adjusted to minimize the radiation in the semispace $z < 0$ and avoid interference with the reflector radiation.

Figure 5 compares the lens radiation patterns given by the CST and the GO approximation calculated from (4). As observed, the main lobe shows good agreement, and the minor differences are due to higher-order modes generated by reflections on the dielectric interface. Due to a small radiation phase error in the main lobe region, we consider a displacement of 0.1 cm in the lens focus towards the negative z-axis. Figure 6 compares the return loss at the horn 50 ohms port with and without the lens.

3. Reflector Shaping

The circularly symmetric reflector surface is illuminated by a spherical wavefront with a phase center at P with a radiation pattern $G_L(\alpha)$, as described by (4), and $\alpha \in [0, \alpha_N]$ defines the tube of rays incident on the main reflector. The reflector generatrix is shaped to radiate a prescribed vertical

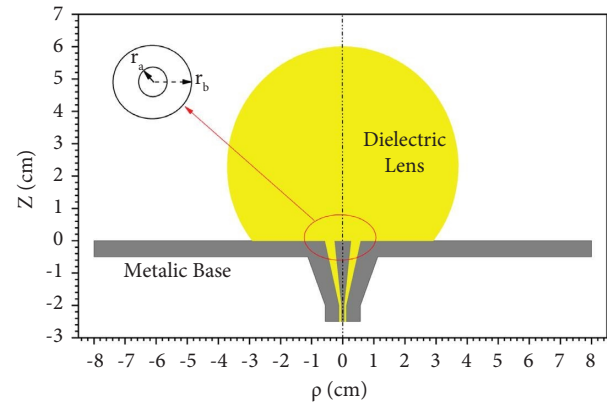

Figure 3: Lens-horn schematic.

pattern $G_B(\beta)$ in the far-field region of the antenna, where β is the direction of observation relative to the z-axis, and $\beta \in [\beta_0, \beta_M]$ defines the tube of rays reflected by the main reflector.

This work follows the GO shaping technique employed in [11], where the generatrix is described by a series of concatenated conical sections $M_m (m = 1,...,M)$, as illustrated in Figure 7. The sections are sequentially concatenated to each other and all of them with one focus at P_0. The angles α_{m-1} and α_m limit the conic section M_m, and its axis has an elevation angle γ_m with respect to the z axis. r_S represents the distance between P and a point at M_m and is expressed as follows:

$$r_m(\alpha) = \frac{a_m}{b_m \sin(\alpha) + (1 + d_m)\cos(\alpha)}, \text{ for } \alpha \in [\alpha_{m-1}, \alpha_m], \quad (7)$$

where

$$a_m = c_m \left(e_m - \frac{1}{e_m}\right),$$
$$b_m = e_m \sin(\gamma_m), \quad (8)$$
$$d_m = e_m \cos(\gamma_m) - 1,$$

and $2c_m$ and e_m are the interfocal and eccentricity of M_m, respectively. By applying the Snells Law of reflection on the polar equation of M_m, one derives the relation between the incident and reflected directions of the ray [11].

$$b_m \left[\cot\left(\frac{\alpha}{2}\right) + \cot\left(\frac{\beta}{2}\right)\right] + d_m \left[\cot\left(\frac{\alpha}{2}\right)\cot\left(\frac{\beta}{2}\right) - 1\right] = 2. \quad (9)$$

The coefficients a_m, b_m, and d_m define the section M_m, and the following iterative procedure obtains them. By using (9), the coefficients b_m and d_m are obtained by imposing the known mapping condition to the rays at the extremes of the section m, $(\beta_{n-1}, \alpha_{n-1})$, and (β_m, α_n). To ensure the continuity of the surface, the value of a_m is obtained from values of r_{Sm-1} and α_{n-1} determined in the previous step $(m - 1)$.

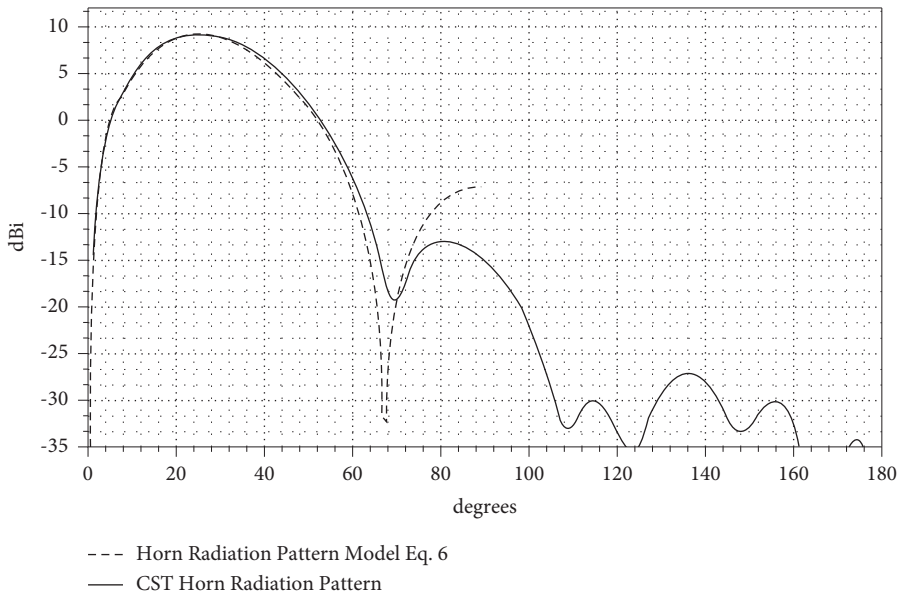

Figure 4: Horn radiation pattern at 30 GHz.

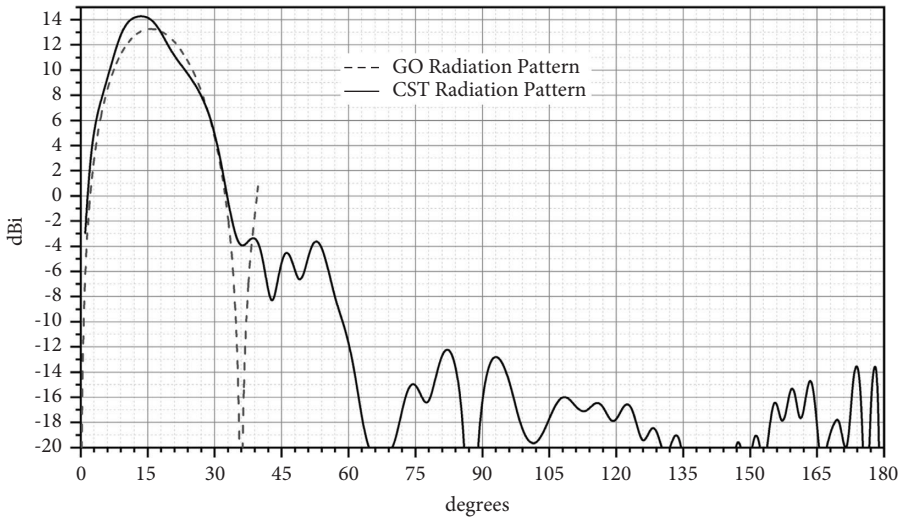

Figure 5: Lens radiation pattern at 30 GHz.

For the first section, the reflector vertex V_0 defines the initial parameter a_1. As observed, the iterative technique requires the previous definition of the relation between the angle α_m and β_m, the angles of the incident, and refracted rays at the extremes of each section, respectively. This relation is obtained by applying the conservation of energy principle within a ray tube that relates the radiated power density incident at the dielectric on the interface and the refracted power density specified in the far-field.

$$\int_{\beta_0}^{\beta_m} G_B(\beta)\sin(\beta)\,d\beta = N_0 \int_{\alpha_0}^{\alpha_m} G_L(\alpha)\sin(\alpha)\,d\alpha. \tag{10}$$

N_0 is the normalization factor to impose energy conservation within the tube of rays emerging from the lens and the far-field coverage. As described in [11], the synthesis technique is fast, and 25 sections can accurately describe the surface for the examples shown in the design.

4. Design Examples

To illustrate the performance of the proposed omnidirectional antenna configuration, we explore the feed lens design described in Section 2 to illuminate two types of circularly symmetric reflectors. Case I considers the reflector obtained by spinning a parabola section around the symmetry axis (z-axis). The parabola focal point is at P at the symmetry axis and coincides with the virtual focus of the rays emerging from the lens interface, as shown in Figure 2. It transforms the spherical wavefront emanating from the point P into a conical wavefront at the antenna aperture (see Figures 1 and 2) and axis pointing at $\beta_0 = 102^\circ$.

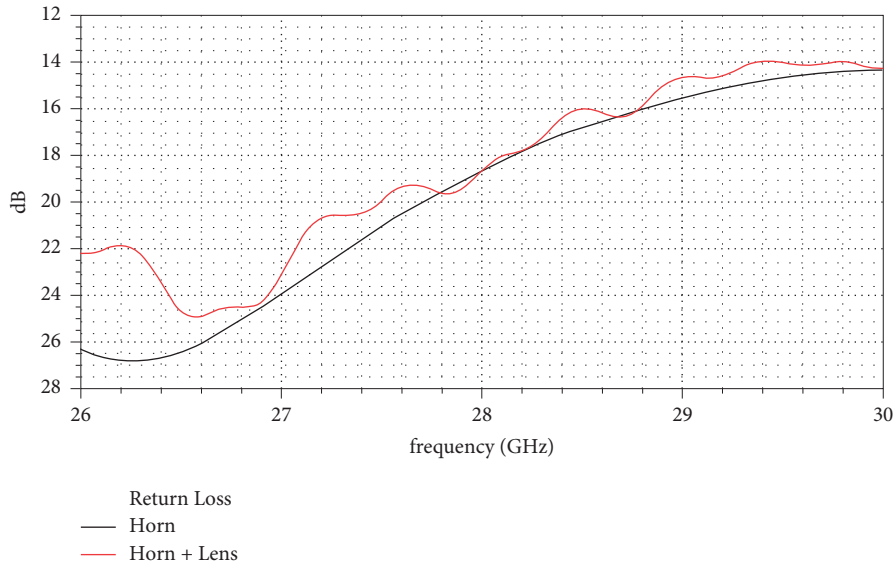

Figure 6: Horn-lens return loss.

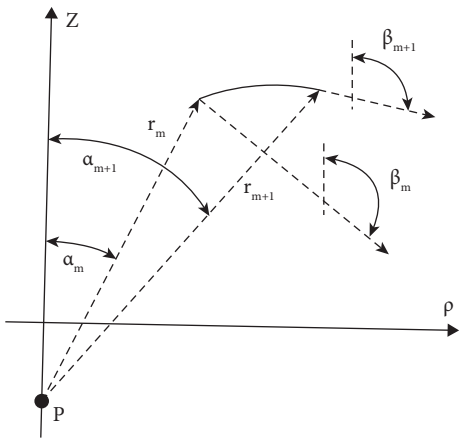

Figure 7: Geometry of the conic section.

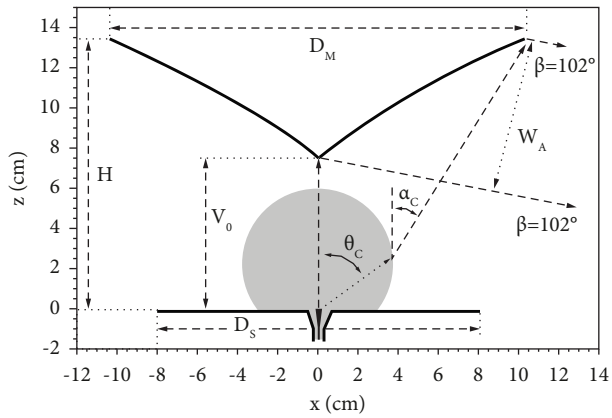

Figure 8: Antenna geometry and basic parameters for case I.

To illuminate the reflector, we consider the rays within the cones with semiangle $\theta_C = 55^\circ$ and $\alpha_C = 31.4^\circ$, which provide a reflector edge illumination lower than −10 dB and minimize the spillover above the horizon. For comparative purposes, the vertex distance from the origin is $V_0 = 7.4$ cm and is adjusted to make the volume of the truncated cone that circumscribes the antenna close to the volume of the Option I design presented in [4]. As illustrated in Figure 8, it yields a parabola with a focal distance of $F = 6.644$ cm, antenna dimensions $D_M = 20.58$ cm, $H = 13.344$ cm, and an aperture width of $W_A = 7.95$ cm, larger than the designs presented in [4]. Table 1 lists the main antenna parameters together with the design options in [4], where is possible to observe that the use of a dielectric lens to illuminate the reflector leads to a smaller high (H) and a larger reflector radius (D_M).

From the results of the CST full-wave analysis, Figure 9 shows the antenna radiation patterns in the vertical plane, and Figure 10 shows a near-field map that helps to understand the radiative behavior of the antenna and estimate

Table 1: Some geometrical parameters and maximum gain of the omnidirectional lens reflector and dual reflector designs [4].

	Option I	Option II	Lens reflector
WA (cm)	7	7	7.95
H (cm)	16.9	17.56	13.45
D_S (cm)	14.7	18.19	16
D_M (cm)	17.8	17.8	20.56
VOLUME (cm^3)	3414	4431	3545
GAIN (dBi)	9.83	11.17	11.12

the interaction with nearby objects [13]. In Figure 10, it is possible to observe the conical wavefront emerging from the reflector towards the $\beta = 102^\circ$ direction. The main lobe has an 11.12 dBi peak radiation pattern at 102.25° and includes the reflection losses at the dielectric interface. Compared to the dual reflector cases in [4], it shows a gain close to the provided by Option II and 1.2 dB higher than Option I design and compactness similar to Option I. The main differences appear in the sidelobe region where the lens

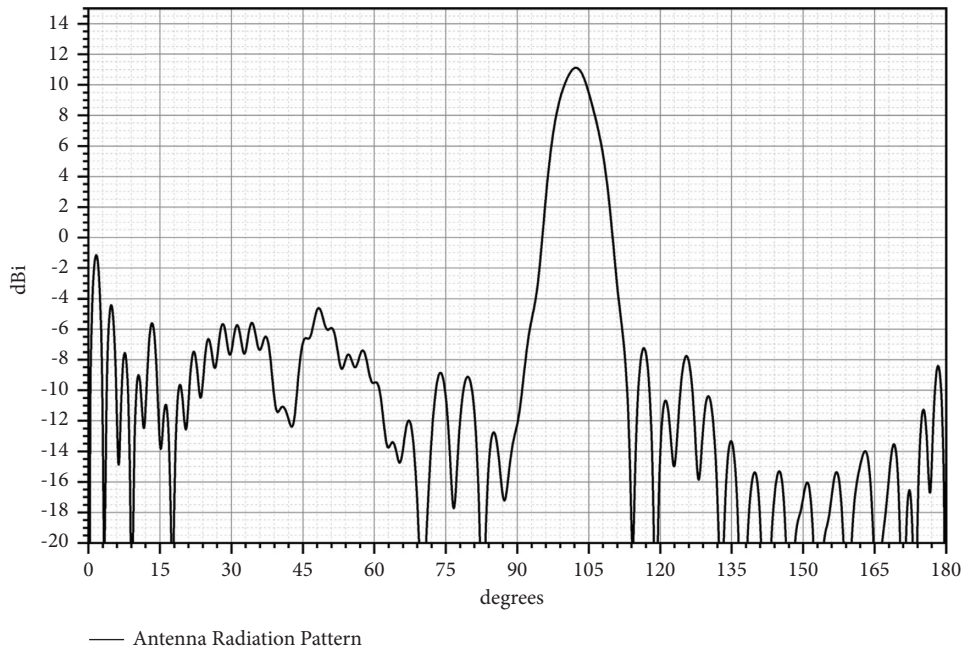

Figure 9: Case I antenna radiation pattern at 30 GHz.

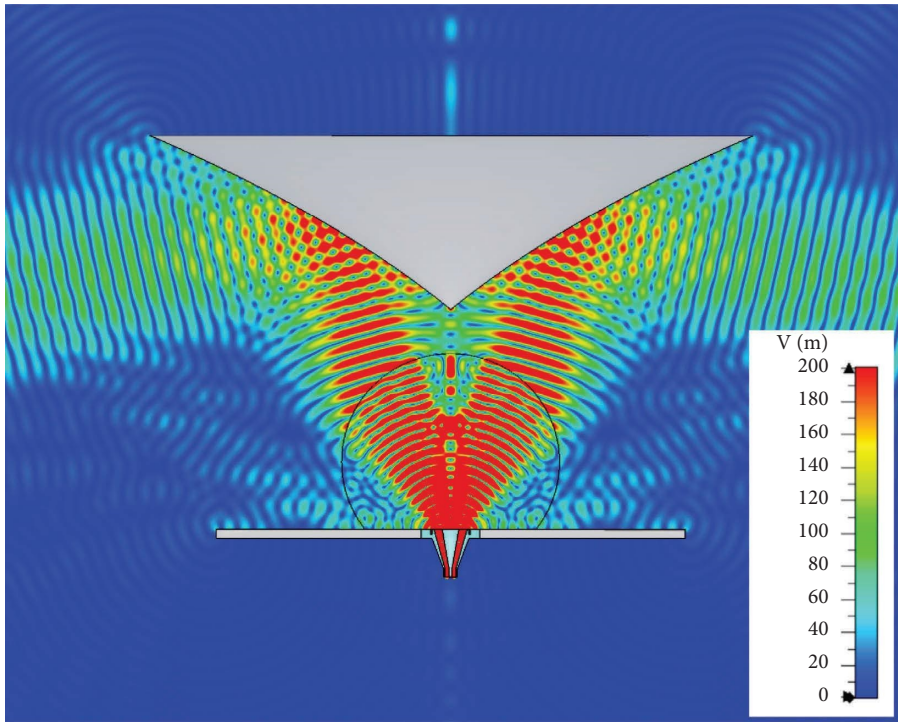

Figure 10: Near-field map of the case I antenna at 30 GHz.

reflector radiation pattern shows lower sidelobe levels close to the z-axis negative, while displaying higher reflector spillover above the horizon.

Case II employs the feed lens system described in Section 2 to illuminate a reflector shaped to generate a cosecant squared radiation pattern $G_B(\beta)$ in the elevation plane. For the reflector synthesis, $G_B(\beta)$ is expressed as follows:

$$G_\beta = G_o \csc^2\left(\beta - \frac{\pi}{2}\right). \tag{11}$$

As observed in Figure 11, the rays emerging from the reflector are concentrated within the space region defined by $95^\circ < \beta < 135^\circ$ in the vertical plane and have a virtual caustic. One critical point of the design is the ray incident at the reflector vertex and reflected in the direction $\beta = 135^\circ$,

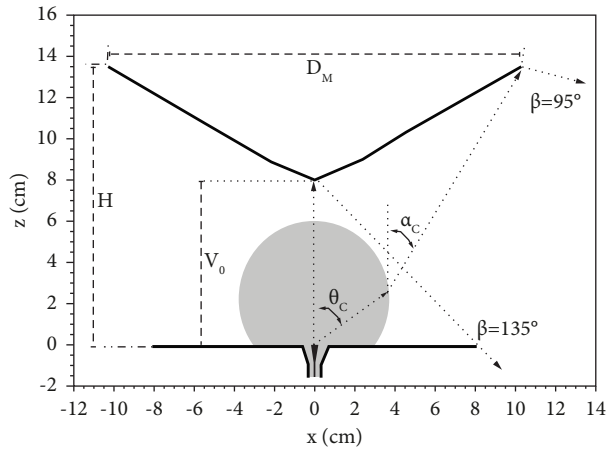

Figure 11: Antenna geometry and basic parameters for case II.

Table 2: Some geometrical parameters of the omnidirectional lens reflector and dual reflector designs [5].

	Case IIA	Lens reflector
H (cm)	16.34	13.36
D_M (cm)	17.8	20.57
D_S (cm)	14.77	16
VOLUME (cm^3)	3401	3528

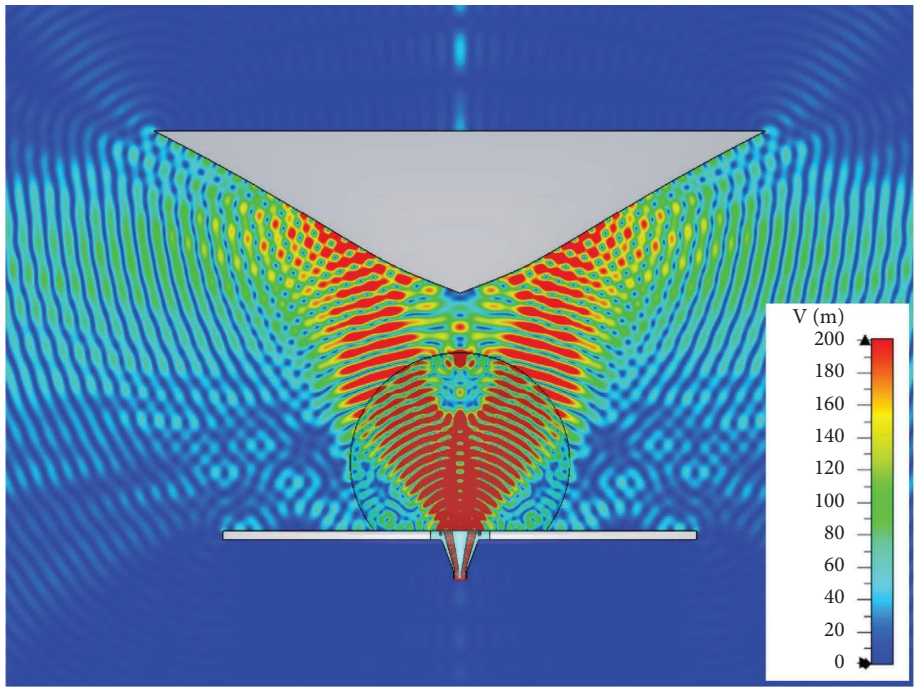

Figure 12: Near-field intensity map of the case II antenna at 30 GHz.

passing close to the dielectric lens and the metallic base. To avoid lens and metallic base blockage in the optical sense and minimize the reflector lens interaction, we move the reflector vertex upwards by making $V_0 = 7.9$ cm, including the horn-lens phase center displacement. The synthesis procedure considers the rays within the cone with a semi-angle $\theta_C = 55^\circ$ to illuminate the reflector, as explained in the previous example. Figure 11 shows the resulting shaped reflector with dimensions $D_R = 20.57$ cm and $H = 13.36$ cm. Table 2 lists the main dimensions of the synthesized antenna

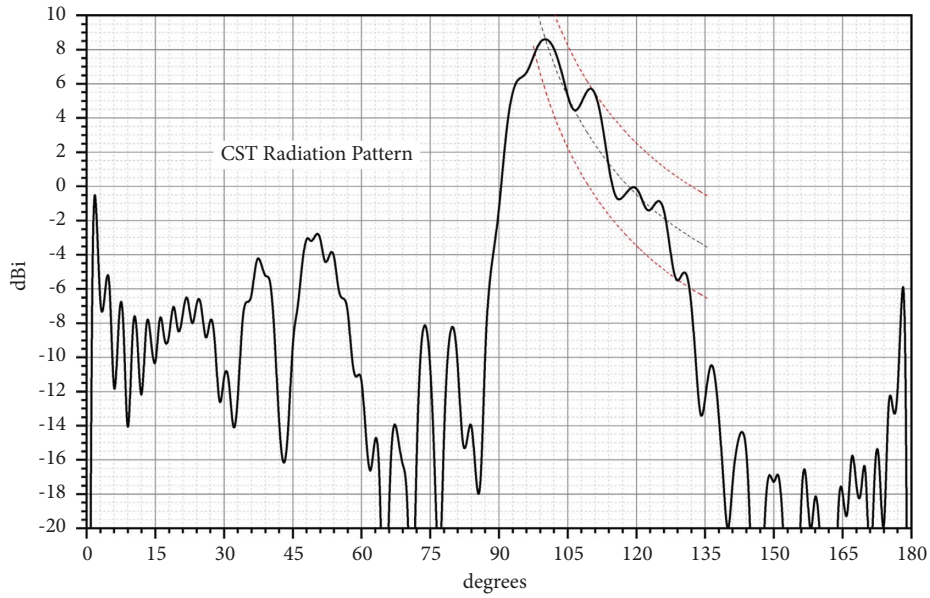

Figure 13: Case II antenna radiation pattern at 30 GHz.

and compares them with the dimensions of Case IIA described in [5].

From the CST analysis, Figure 12 shows the near-field map and Figure 13 shows the antenna radiation pattern. It is observed a peak directivity of 9.16 dBi at $\beta = 99^{\circ}$ and small oscillations around the desired cosecant-squared pattern due to the interaction of the lens fields with those emerging from the reflector. Different from the previous case, the wavefront emerging from the reflector shows a curvature to generate the cosecant-squared radiation pattern. Compared with the omnidirectional dual reflector shaped for a cosecant-squared radiation pattern, using a lens allows the design for compacter configuration [5], as observed in Table 2, and it also avoids the grazing incidence when the main reflector is placed below the feed-subreflector system, as observed in [5].

5. Conclusions

The paper has explored an omnidirectional antenna configuration composed of a reflector fed by a shaped dielectric lens associated with a coaxial TEM horn for vertical polarization. For LMDS applications around 30 GHz, two successful design examples were presented and analyzed using a full-wave approach. They showed results comparable to other types of omnidirectional antenna configurations. For each case, geometrical limitations were outlined, such as compactness and the conditions to avoid lens blockage.

Appendix

A. Lens Geometry

The rays emitted by a point source at the origin refracts on the lens interface and produces a spherical wavefront with a center at the virtual focus at $P(0, -Z_0)$. By applying Fermat's principle to the ray path from the origin to the dielectric interface, it has to satisfy the following equation:

$$r_p(\theta) = r_0(\theta)n - c, \tag{A.1}$$

where $r_p(\theta)$ and $r_0(\theta)$ are the distances of the interface points from the origin and the point $P(0, -Z_0)$,respectively, as described in Figure 2. The triangle defined by the points OPS satisfies the following relation:

$$Z_0^2 + r_0^2(\theta) + 2r_0(\theta)Z_0\cos(\theta) = r_p^2. \tag{A.2}$$

The combination of these two equations results in the following expression:

$$Z_0^2 + r_0^2(\theta) + 2r_0(\theta)Z_0\cos(\theta) = \left[nr_0(\theta)\right]^2 + c^2 - 2\mathrm{ncr}_0(\theta). \tag{A.3}$$

The solution of the abovementioned equation yields the following expression for the function $r(\theta)$:

$$r_0(\theta) = \frac{nc + Z_0\cos(\theta)}{\left(n^2 - 1\right)} \pm \frac{\sqrt{\left[nc + Z_0\cos(\theta)\right]^2 + \left(Z_o^2 - c^2\right)\left(n^2 - 1\right)}}{\left(n^2 - 1\right)}. \tag{A.4}$$

B. Horn Radiation Pattern

The expression (6) can be obtained by computing the radiated field of an annular aperture with inner radius r_a and outer radius r_b, and illuminated by the TEM mode (see Figure 2 in [13]). For the task, the aperture fields are replaced by equivalent magnetic current on the annular aperture:

$$\overrightarrow{M}(\rho', \varphi') - \hat{\imath}_z \times \overrightarrow{E}_{\mathrm{TEM}}\left(\rho', \varphi'\right) = \left[\frac{E_0}{\rho'}\right]\hat{\imath}_{\varphi}. \tag{B.1}$$

The electric vector potential in the far-field region is calculated by integrating the magnetic aperture currents

$$\vec{F}(\vec{r}) \approx \frac{\varepsilon}{4\pi}\frac{e^{-ikr}}{r}\int_{r_i}^{r_e}\int_{0}^{2\pi}\vec{M}_S\left(\rho', \varphi'\right)e^{ik\rho'\,\mathrm{sen}(\theta)\cos(\varphi-\varphi')}\rho'\,\mathrm{d}\rho'. \tag{B.2}$$

The electric vector potential has an azimuthal component given by

$$F_\varphi = \frac{\varepsilon}{4\pi}\frac{e^{-ikr}}{r}\int_{r_i}^{r_e}\int_{0}^{2\pi}\left[\frac{E_0}{\rho'}\right]\cos\left(\varphi'\right)e^{ik\rho\,\mathrm{sen}(\theta)\cos(\varphi')}\rho'\,\mathrm{d}\varphi'\,\mathrm{d}\rho. \tag{B.3}$$

The analytical solution of the integrals yields the following expression for the component

$$F_\varphi = \frac{\varepsilon i E_0}{2k}\frac{e^{-\mathrm{ikr}}}{r}\left[\frac{J_0\left(kr_e\sin(\theta)\right)}{\sin(\theta)} - \frac{J_0\left(kr_i\sin(\theta)\right)}{\sin(\theta)}\right], \tag{B.4}$$

and the electric field in far-field region given by

$$E_\theta = -i\omega\eta F_\varphi = \frac{E_0}{2}\frac{e^{-\mathrm{ikr}}}{r}\left[\frac{J_0\left(kr_e\sin(\theta)\right)}{\sin(\theta)} - \frac{J_0\left(kr_i\sin(\theta)\right)}{\sin(\theta)}\right]. \tag{B.5}$$

Data Availability

All data supporting the results were generated during the study.

Conflicts of Interest

The authors declare that they have no conflicts of interest.

Acknowledgments

This work was partially supported by CAPES, grant no 068419/2014-01.

References

[1] P. Besso, R. Bills, P. Brachat, and R. Vallauri, "A millimetric wave omnidirectional antenna with cosecant squared elevation pattern," in *Proc. 10th Int. Conf. Antennas Propagation (ICAP)*, vol. 1, pp. 448–451, Edinburgh, UK, April 1997.

[2] A. G. Pino, A. M. A. Acuña, and J. O. R. Lopez, "An omnidirectional dual-shaped reflector antenna," *Microwave and Optical Technology Letters*, vol. 27, no. 5, pp. 371–374, 2000.

[3] A. Kezuka, Y. Kazama, and Y. Yamada, "Antennas with Cosecant Square Radiation Pattern Both Upward and Downward for FWA," in *Proceedings of the IEEE Antennas and Propagation Society International Symposium*, pp. 782–785, Columbus, OH, USA, June 2003.

[4] F. da Silva Moreira and J. R. Bergmann, "Axis-displaced dual-reflector antennas for omnidirectional coverage with arbitrary main-beam direction in the elevation plane," *IEEE Transactions on Antennas and Propagation*, vol. 54, no. 10, pp. 2854–2861, 2006.

[5] J. R. Bergmann and F. J. S. Moreira, "Omnidirectional ADE antenna with a GO-shaped main reflector for an arbitrary far-field pattern in the elevation plane," *IET Microwaves, Antennas & Propagation*, vol. 3, no. 7, p. 1028, 2009.

[6] J. Lee, "Dielectric lens shaping and coma-correction zoning, Part I: analysis," *IEEE Transactions on Antennas and Propagation*, vol. 31, no. 1, pp. 211–216, 1983.

[7] C. A. Fernandes and L. M. Anunciada, "Constant flux illumination of square cells for millimeter-wave wireless communications," *IEEE Transactions on Microwave Theory and Techniques*, vol. 49, no. 11, pp. 2137–2141, 2001.

[8] B. Chantraine-Bares, R. Sauleau, L. Le Coq, and K. Mahdjoubi, "A new accurate design method for millimeter-wave homogeneous dielectric substrate lens antennas of arbitrary shape," *IEEE Transactions on Antennas and Propagation*, vol. 53, no. 3, pp. 1069–1082, 2005.

[9] B. S. Westcott and F. Brickell, "General dielectric-lens shaping using complex co-ordinates," *IEE Proceedings H Microwaves, Antennas and Propagation*, vol. 133, no. 2, p. 122, 1986.

[10] R. E. Collin and F. J. Zucker, *Antenna Theory, Part 11*, McGraw-Hill Book Co., Inc, New York, NY, USA, 1969.

[11] R. A. Penchel, S. R. Zang, J. R. Bergmann, and F. J. S. Moreira, "GO shaping of omnidirectional dual-reflector antennas with arbitrary main-Beam Direction in Elevation Plane by Connecting Conic Sections," *IJAP*, vol. 2018, Article ID 1409716, 9 pages, 2018.

[12] S. Zang and J. R. Bergmann, "Analysis of omnidirectional dual-reflector antenna and feeding horn using method of moments," *IEEE Transactions on Antennas and Propagation*, vol. 62, no. 3, pp. 1534–1538, 2014.

[13] R. Cicchetti, O. Testa, and D. Caratelli, "A numerical procedure for the analysis of EMC/EMI problems in radio communication systems operating in complex environments," *IEEE Transactions on Electromagnetic Compatibility*, vol. 54, no. 6, pp. 1269–1280, 2012.